Journal of Molecular Structure 1184 (2019) 114–122

Contents lists available at ScienceDirect

Journal of Molecular Structure

journal homepage: http://www.elsevier.com/locate/molstruc

Terahertz spectroscopy of diglycidylether of bisphenol A: Experimental investigations and density functional theory based simulations

P. Suma Sindhu [a], Dipak Prasad [a], Simone Peli [b], Nilanjan Mitra [a, *], P.K. Datta [a]

[a] Indian Institute of Technology Kharagpur, Kharagpur, 721302, India
[b] Elettra Sincrotrone Trieste, Province of Trieste, 34149, Italy

ARTICLE INFO

Article history:
Received 5 November 2018
Received in revised form
2 January 2019
Accepted 29 January 2019
Available online 8 February 2019

ABSTRACT

A combined methodology of Terahertz spectroscopy and Density functional theory based simulations is presented for a molecule to determine its molecular vibration frequency and associated configuration. A case study of diglycidylether of bisphenol A, which is an important ingredient of epoxy resin, has been presented in this manuscript. Apart from determination of absorbtion peaks in the THz regime both through experiment and simulation, the vibration configuration corresponding to each of the peaks are also presented. Within 3 THz, the refractive index of the material is determined to be within 1.15−1.3 and the dielectric constant is estimated as 1.5.

© 2019 Published by Elsevier B.V.

1. Introduction

Vibration of entire molecule as well as intermolecular vibrations is usually determined at very low wavenumbers, typically below 100 cm^{-1}. Far infrared spectroscopy of a molecule is unable to probe these regimes; Raman spectroscopy can probe these regimes but it should be realized that molecular vibrations stimulated in the Raman process may not necessarily be the same as those excited by the absorption of infrared light [1]. In a molecule having a centre of symmetry, Raman active transitions are IR inactive and IR active modes are inactive in Raman. Thereby one of the most commonly used methodologies to probe these frequency regimes where the entire molecule vibration and/or the intermolecular vibration is predominant is through Terahertz (THz) spectroscopy [2,3]. It should be understood that determination of the entire molecule vibration is many a times required than the determination of a specific bond stretch or angle vibrations. An example where the entire molecular vibration may be necessary to be determined is in determination of tacticity in different polymeric materials [4].

THz absorption spectroscopy can be performed experimentally as well as determined numerically through density functional theory calculations. In this manuscript both experimental and numerical methodologies of spectroscopic determinations are presented for an epoxy material: Diglycidylether of bisphenol A (DGEBA). DGEBA is a glycidyl epoxy marked by the presence of aromatic and oxirane rings. It is one of the most widely used glycidyl epoxies which are synthesized by the addition of epichlorohydrine and bisphenol A. It should be noted that epoxy resin is widely used for different applications ranging from aerospace, marine to even infrastructure. Typically, the final epoxy resin product (a thermoset polymer developed as a result of crosslinking of the epoxy base with the hardener) consists of an epoxy base (such as DGEBA) along with a hardener. Various choices of hardener are possible for a particular type of epoxy base depending upon the desired properties for the application.

The molecular structure of DGEBA typically consists of aromatic rings and oxirane groups (detailed representation of which can be obtained from Fig. 1). Due to presence of large amount of hydroxyl groups, these epoxies have high viscosities. The linkage between the aromatic ring and the oxygen (ether) in DGEBA has a strong electron-withdrawing effect which makes the oxirane group highly reactive towards nucleophilic compounds (like amines). Thereby the best performance and highest cross-linking degree for DGEBA-based epoxies are achieved when cured via an addition mechanism with diamines (either aliphatic or aromatic). However, it should be noted that our objective in this study is not on the curing process of these epoxies along with hardener to yield a 3D cross-linked epoxy resin material. Our scope of work in this study is to concentrate on

* Corresponding author.
E-mail address: nilanjan@civil.iitkgp.ac.in (N. Mitra).

https://doi.org/10.1016/j.molstruc.2019.01.094
0022-2860/© 2019 Published by Elsevier B.V.

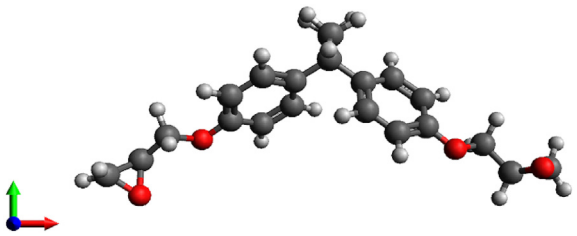

Fig. 1. Molecular structure of DGEBA (black: Carbon; grey: Hydrogen; red: Oxygen).

the spectroscopic signatures of DGEBA at the terahertz regime which typically correspond to molecule vibrations. In this regard, it should be noted that there are numerous studies in literature which focuses on midIR and nearIR ($100 - 4000\ cm^{-1}$) spectroscopy of the material, which have been referenced in the following paragraph but there are no spectroscopic study at the terahertz frequencies for the material in existing literature. Apart from experimental investigation of the material in the THz range, Density functional studies have also been carried out to explain the peak position of the experimental observations and the nature of vibration.

The characteristics absorption of the oxirane ring in the midIR region has been identified at $915\ cm^{-1}$ which is typically attributed to the C—O deformation along with some unknown processes [5]. Another absorption band of the oxirane ring is located at $3050\ cm^{-1}$ which can be attributed to the C—H tension of the methylene group. However, because of close proximity of the band to the strong O—H absorptions, it is difficult to identify and assign this band. In the near IR region, the absorbtion bands related to the oxirane groups are $4530\ cm^{-1}$ (corresponding to combination band of the second overtone of the epoxy ring stretching with the fundamental CH stretching at $2725\ cm^{-1}$) [6] and $6070\ cm^{-1}$ (corresponding to first overtone of terminal CH_2 stretching mode) [7]. The main focus in these IR spectroscopic studies was on identifying the presence of oxirane ring through its different modes of possible vibrations, since the presence of oxirane group is a typical characteristic of the molecule. Other detailed identification of the band in the mid and near IR regimes and their corresponding assignment for DGEBA molecule can be found in literature [8].

The entire molecular vibration of the structure has not been probed previously in literature which is the main focus in this study. It should be noted that this type of entire molecular motion typically happens at very low frequency range (less than $100\ cm^{-1}$) and can be characterized as spectroscopic signatures in the THz regime. In an analogy, this type of macro-molecular vibrations are similar to that of phonon vibrations in periodic structures in crystals. It should also be noted at this point that intermolecular vibrations may also lead to low frequency range vibrations. However, in our numerical study we have only considered a single molecule and thereby the numerical study has a limitation in its inability to account for intermolecular vibrations which might be observed in experimental investigations using THz spectroscopy.

2. Methodology

2.1. Experimental investigations

The terahertz spectroscopy setup that has been used for this experiment is given in Fig. 2. Terahertz (THz) time domain spectroscopy (TDS) measures the THz electric field in transmission mode of a sample with respect to a reference. The Fourier transform of the time domain data results in amplitude and phase of the transmitted THz wave spectra. THz radiation is provided in pulses with almost single cycle oscillation of the electric field for a duration of about 1 ps. THz pulses are generated and detected using ultra short pulses (80 fs) from Ti:Sapphire laser with a central wavelength of around 800 nm and repetition rate of 1 kHz. The output power of the laser beam is 2.7 W with an energy of 2.7 mJ per pulse; a small part of which is used for THz generation and detection. In order to obtain an optimal configuration for the THz generation, the size of the laser beam is reduced down to 2.0 mm from 9.0 mm using a telescope composed of two lenses of focal length 15 cm and 5 cm. A beam splitter is used to split the beam into two parts, one part with power < 20 mW is used as pump to generate THz and the other part, with power 0.5 μW, is used as probe to detect THz. The THz radiation is generated through the process of second order nonlinear optical rectification in a ZnTe (110) crystal of thickness 1 mm. THz is generated when the optical beam is incident on first ZnTe crystal. Thick (1 mm) crystals are used to generate high power THz radiation due to longer interaction length between light and material, however bandwidth is limited to maximum of 3 THz. The THz radiation is collected by a 6 inches focal length and gold coated parabolic mirror and is driven onto a second parabolic mirror of the same focal length. The role of this second parabolic mirror is to focus the THz radiation on the sample, that is placed between second and third parabolic mirrors. The transmitted THz wave from sample is then driven onto the fourth parabolic mirror that focuses it on the detection crystal, where it is coherently detected by electro-optic sampling in a second ZnTe crystal of thickness 0.5 mm. A motorized delay stage (Newport Corp. USA Model No. GTS 150) with delay resolution of 0.67 fs is used to introduce delay between THz and optical probe pulse. A computer controls the delay lines and records data from the lock-in amplifier, which is coupled to an optical chopper for improving the signal-to-noise ratio by phase sensitive detection. The pump beam is chopped at an optimized chopper frequency of 253 Hz. THz is indirectly detected exploiting the birefringence of the detection crystal that, under the effect of the electric field of the THz radiation, induces a variation of phase in the vertical and horizontal polarization components of the probe light. This variation is measured by an optical balanced detector (OBD) (Newark Corp. Japan, Model type: NDT-40110GTP). Inside the detector system, a polarizing beam splitter separates the vertical and horizontal components of the polarization of the probe light and send them on two different slow photodiodes. In the absence of THz, the OBD is rotated to obtain equal intensity in the two photodiodes. The difference of the photodiode signal will be read as null in lock-in amplifier. In the presence of THz, polarization of beam is changed to elliptical due to electro-optic effect: this makes the lock-in amplifier to read a non-zero value. The setup is placed in a plexiglass box and nitrogen gas is sent into the box to avoid absorption of THz by water molecules present in air.

2.2. Sample preparation

Liquid DGEBA (commercially available as Araldite CY 230) is placed in a plastic and is spread evenly using spatula. Another plastic sheet is placed on it and is compressed such that there are no air voids in between the plastics. Reference cell for DGEBA is prepared by joining two plastic plates without any space in between. The plastics with DGEBA is fixed to the holder and is placed carefully on the mount. Thickness of sample is 280 μm as measured by electronic vernier calipers which is also verified by the measurement of delay occurring in transmission of THz pulse through the sample.

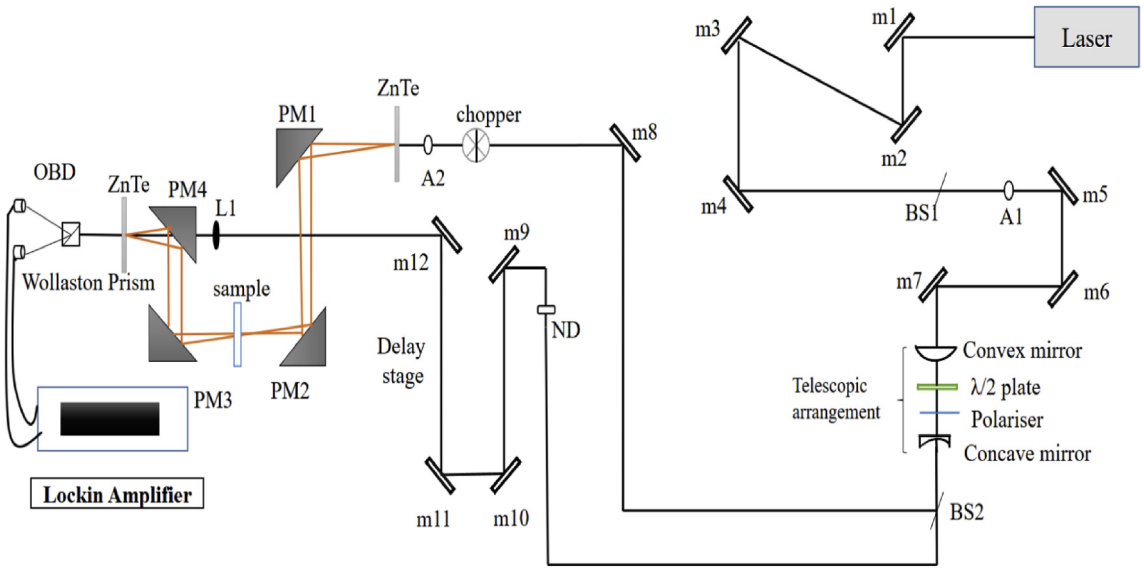

Fig. 2. Terahertz Spectroscopy setup (BS Beam Splitter,A-Aperture,m-mirror,L-lens,ND-neutral density filter,PM-parabolic Mirror,OBD-Optical Balanced Detector).

2.3. Numerical investigations

Density functional theory calculations have been performed on the DGEBA molecule in Gaussian 09 software [9]. Hybrid functional B3LYP (which is based on mixing the exact exchange from Hartree-Fock theory with the rest of the exchange correlation part from Density Functional theory) has been utilized for this study [10–12]. Gaussian type basis set has been used. Two different basis set has been used for obtaining the absorption spectra: 6-31G (d) and 6-311G (dp++) (where 6 refers to Gaussian type orbitals (GTO) defined for the core orbital, 3 GTO for the inner valance and 1 GTO for the outer valence, in case of 11 there are 2 GTO for the outer valence). Polarization has also been added to the atomic orbitals so that they can distort from their original shape under the influence of surroundings: (d) represents polarization added as d-type functions for non-Hydrogen atoms whereas (pd) represents p type functions for the hydrogen atoms and d-type for other non-Hydrogen atoms. The Pople basis set can also be made diffuse in which the electrons are allowed to move far away from the nucleus creating diffuse orbitals: in this case the term ++ refers to diffuse functions being added on to all atoms. Note in here, the 6-31G(d) is one of the most basic type of basis functions whereas 6-311G (dp++) represents one of the most advanced basis sets. These two basis sets were used to determine if there is any significant difference in the absorption spectra obtained for the molecule.

The potential energy surface of the material is obtained through perturbation analysis of the molecule. Hessian matrix (second derivative of the potential energy with respect to atomic positions) is eventually used to obtain the forces. Diagonalization of the Hessian matrix is utilized to determine the eigenvalues of the system which typically determines the vibrational frequencies of the molecule.

3. Results and discussion

3.1. Experimental data analysis

Time domain of THz field after passing through the sample and plastic reference is shown in Fig. 3a) along with the FFT of the time domain data (refer Fig. 3b). Echoes has been removed from the sample results so that the Fabry-Perot effect can be neglected. Apart from removing the reflection, it should also be noted that the thickness of the sample taken (280 μm) is of same order of the spatial length of THz pulse (300 μm); hence FP mode can be ruled out in our case.

The complex FFT transmission data of sample is compared to that of reference (plastic) in following manner:

$$\frac{\psi_s}{\psi_r} = \rho(\omega)e^{-i\phi(\omega)} \tag{1}$$

where ψ_s and ψ_r are complex FFT of sample (DGEBA) and reference (plastic) respectively. The real part of the refractive index n_s and imaginary part of the refractive index k_s (represented in Fig. 4) can be written in terms of $\phi(\omega)$ and $\rho(\omega)$ as follows [13]:

$$n_s(\omega) = \phi(\omega)\frac{c_0}{\omega d} + 1 \tag{2}$$

$$k_s(\omega) = ln\left(\frac{4n_s(\omega)}{\rho(\omega)(n_s(\omega)+1)^2}\right)\frac{c_0}{\omega d} \tag{3}$$

where c_0 is the speed of light and d is the sample thickness.

As can be observed the real part of the refractive index varies between 1.15 and 1.3 demonstrating that the material is transparent in the THz regime. Based on literature [14] DGEBA can be classified as a low loss (and/or a non-polar) polymer having refractive index < 1.55. It should be mentioned that it has been reported that the average refractive index is 1.34 for Bisphenol A (one of the components of DGEBA, the other being epichlorohydrin) in 0.2–2 THz range [15].

The imaginary part of refractive index k_s, is related to absorption coefficient $\alpha(\mathrm{cm}^{-1})$) (shown in Fig. 5) as

$$\alpha(\omega) = \frac{2}{d}ln\frac{4n_s(\omega)}{\rho(\omega)(n_s(\omega)+1)^2} \tag{4}$$

The complex dielectric constant and complex refractive index have generalised Maxwell's relation [16]:

$$\varepsilon = [n(\omega)]^2 \tag{5}$$

which can be expressed as

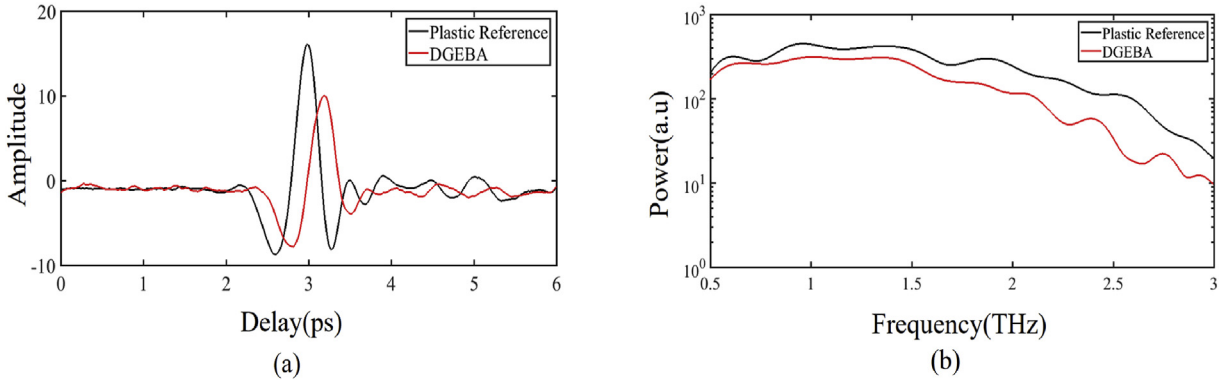

Fig. 3. (a) Time domain data of the THz field through the sample (b)FFT of time domain data.

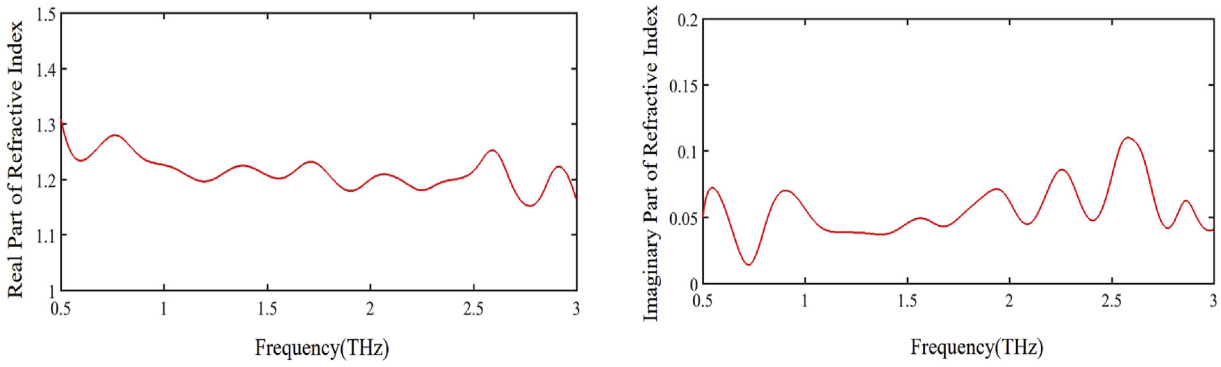

Fig. 4. Real and Imaginary part of refractive index of DGEBA.

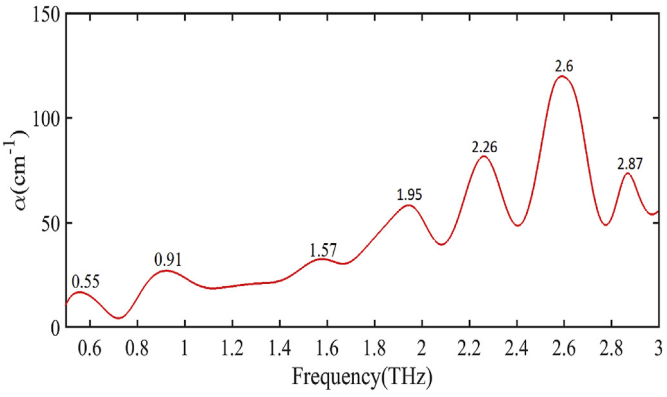

Fig. 5. Absorption Coefficient of DGEBA obtained experimentally.

$$n(\omega)^2 - k(\omega)^2 - 2jn(\omega)k(\omega) = \varepsilon' - i\varepsilon'' \tag{6}$$

and Real and imaginary parts of dielectric constants are determined from the following equations

$$\varepsilon(\omega) = \varepsilon_s'(\omega) + i\varepsilon_s''(\omega) \tag{7}$$

where

$$\varepsilon_s'(\omega) = n_s(\omega)^2 - \left(\frac{c_0 * \alpha(\omega)}{2\omega}\right)^2 \tag{8}$$

and

$$\varepsilon'(\omega) = 2n_s(\omega)k_s(\omega) \tag{9}$$

Dielectric constant for the material is estimated from Fig. 6 as 1.5. It should be noted that the dielectric constant of the material can change at different climatic exposure conditions (such as heat, cold, UV exposure etc). The data about dielectric constant that is being provided in here can serve as a reference to that of a control sample in those studies.

3.2. DFT simulation results

The peak frequency positions (as obtained using two types of basis functions) are show in Fig. 7. It should be noted that DFT calculation of integrated absorption coefficient (done with Gaussian09) is based on napierian absorbance i.e. $\log_e \frac{I_0(\nu)}{I(\nu)}$ where $I_0(\nu)$ and $I(\nu)$ are intensities of incident and transmitted radiation respectively. The IR intensity obtained from DFT simulation is in form of integrated absorption coefficient A (Km/mole) [17], which can be related to the absorption coefficient $\alpha(cm^{-1})$ in following manner:

$$A = \int \varepsilon(\nu)\, d\nu \tag{10}$$

where $\varepsilon(\nu)$ is molar absorption coefficient related to α as

$$\varepsilon(\nu) = \frac{\alpha}{C} = \frac{1}{Cd}\log_{10}\frac{I_0(\nu)}{I(\nu)} \tag{11}$$

where C is concentration in molarity, d is thickness of sample in cm.

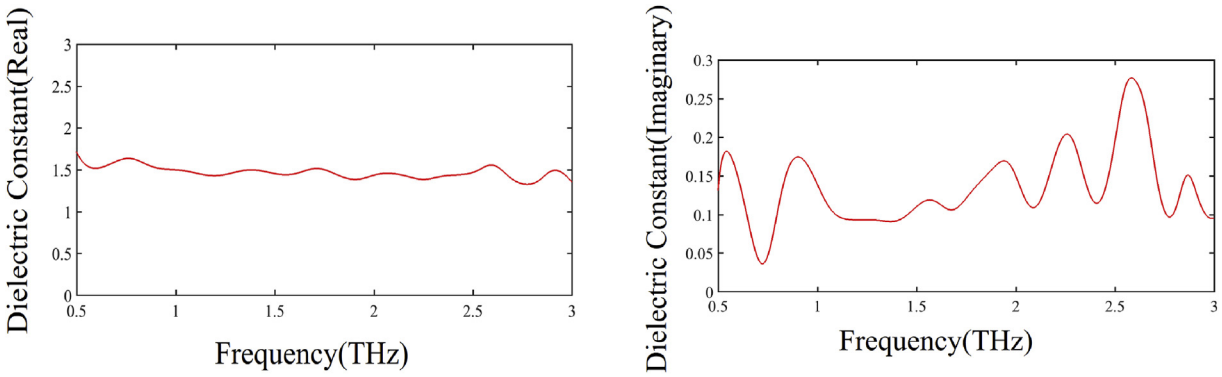

Fig. 6. Real and Imaginary part of Dielectric Constant of DGEBA.

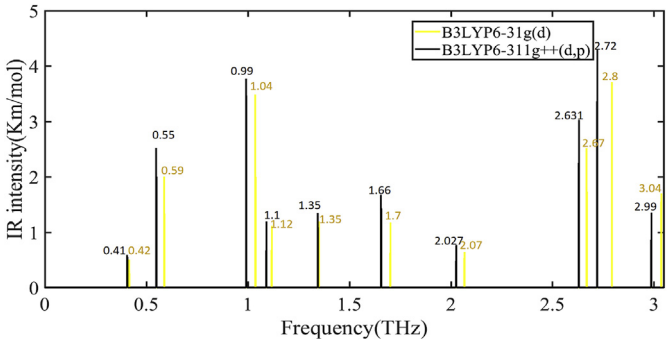

Fig. 7. Absorption Coefficient of DGEBA obtained through DFT calculations.

Since single molecule is being simulated, no effort has been made to convert the napierian absorbance to absorbtion coefficient involving thickness of sample and molarity. Although DFT calculation provides integrated absorption coefficient at particular frequencies in discrete manner, calculation of molar absorption coefficient involves suitable assumption of bandwidth w: $\varepsilon_{max} = \frac{2A}{\pi w}$. However, it should be noted that incorporation of the bandwidth does not change the peak positions, which is why no effort has been made for this type of conversion.

Considering the abscissa or the x-axis of the plot, reasonable correlation could be obtained between experimentally observed absorption spectra in the THz range to that of the numerically simulated one. The differences that are observed between the experimentally observed and the numerically simulated data may be due to the following reasons:

- The sample in the experiment (obtained from commercial sources) may have defects in the molecular structure which may be voids, inclusions and/or exclusions. The sample might even have other materials in trace quantities along with DGEBA as the main component which are undisclosed company secrets. It is quite expected that presence of these materials will alter the absorption spectra in the THz range which probes the molecular motion/vibration rather than bond motion/vibration (as done in IR studies).
- The numerical investigations contain only one molecule of the compound. The presence of other similar molecules might change the intermolecular vibration dynamics of the material which are not accounted for in these simulation studies.

The THz frequency peaks, as observed in numerical simulations typically correspond to different types of molecular vibrations which has been enumerated in the following subsections. The THz frequencies corresponding to 6-311G (dp++) have been highlighted in the subsections for discussions and suitable links have been made with experimental observations and numerical simulations using 6-31G(d) basis set. The two diagrams in each frequency set correspond to two extreme vibration configurations superposed over the initial configuration (shown in grey in the background).

3.2.1. 0.41 THz

The motion corresponds to scissoring of entire molecular structure about the blue axis (axis perpendicular to the plane of the paper). This numerically observed frequency could not be observed in the experimental investigation because of limitations of data reliability in the low frequency ranges of our test setup (note the

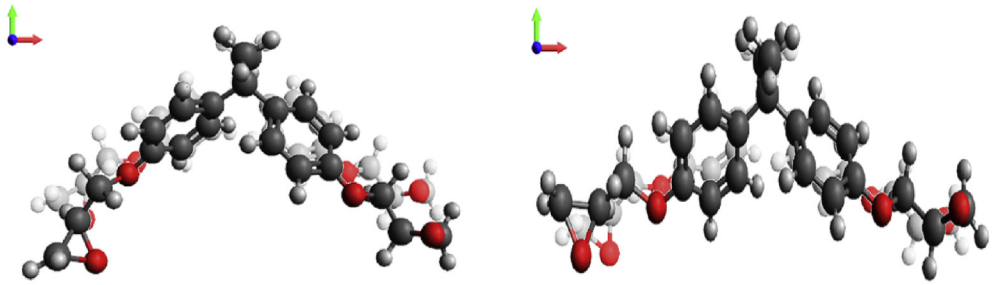

Fig. 8. 0.41 THz vibration configurations. Extremes of the deformed configurations are shown in bold and the initial undeformed configuration is shown in grey (in the background). Supplementary file (video 1) shows the animation of the molecules at 0.41 THz.

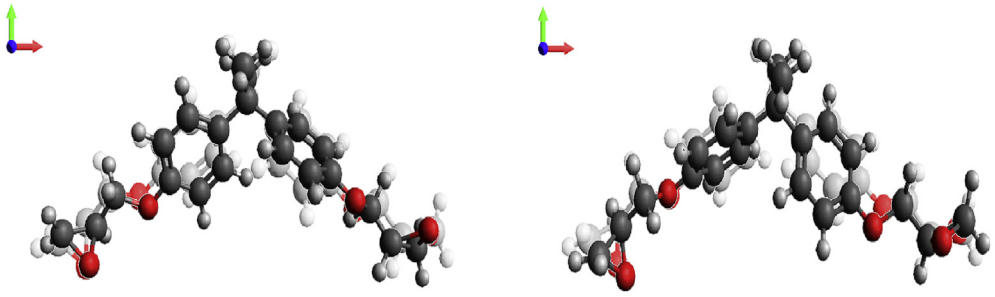

Fig. 9. 0.55 THz vibration configurations. Extremes of the deformed configurations are shown in bold and the initial undeformed configuration is shown in grey (in the background). Supplementary file (video 2) shows the animation of the molecules at 0.55 THz.

starting frequency corresponds to 0.5 THz). Corresponding frequency obtained for the 6-31G(d) basis set is almost the same as that shown in the figure for the other basis function.

Supplementary video related to this article can be found at https://doi.org/10.1016/j.biomaterials.2019.01.017.

3.2.2. 0.55 THz

The motion corresponds to symmetric (and simultaneous) in-out motion of aromatic and oxirane ring about the blue axis. This can also be described as a symmetric torsional mode along the red axis. Projected figure on the plane of the paper shows deformed configuration of the aromatic ring on the two backbone legs of the molecule. Similar type of motion is observed at 0.59 THz for the 6-31G(d) basis set. This frequency matches well with the experimentally observed frequency of 0.55 THz as shown in Fig. 5.

Supplementary video related to this article can be found at https://doi.org/10.1016/j.biomaterials.2019.01.017.

3.2.3. 0.993 THz

The motion corresponds to asymmetric (and alternate) in-out motion of aromatic and oxirane ring about the blue axis. This can also be described as asymmetric torsional mode along the red axis. Similar type of motion is observed at 1.04 THz for the 6-31G(d) basis set. This observed frequency corresponds to 0.91 THz observed experimentally in Fig. 5.

Supplementary video related to this article can be found at https://doi.org/10.1016/j.biomaterials.2019.01.017.

3.2.4. 1.09 THz and 1.35 THz

The motion in 1.09 THz (refer Fig. 11) can be described as a combination of bending and twisting modes of aromatic and oxirane rings in which the twisting is dominant (see Figs. 8–10). For the case of 6-31G(d) basis set it is observed at 1.119 THz.

Supplementary video related to this article can be found at https://doi.org/10.1016/j.biomaterials.2019.01.017.

The motion in 1.35 THz (refer Fig. 12) can be described as a combination of bending and twisting modes of aromatic and oxirane rings in which the bending is dominant. For the case of 6-31G(d) basis set it is observed at 1.351 THz. The peaks for 1.09 and 1.35 are not explicitly observed in the experimental plots (refer Fig. 5) but the combination of these two peaks can provide an explanation to the increasing trend of the plane curve in this frequency domain (see Figs. 14–17).

Supplementary video related to this article can be found at https://doi.org/10.1016/j.biomaterials.2019.01.017.

3.2.5. 1.66 THz

Asymmetric twisting along with slight bending of aromatic and oxirane rings can be observed for this frequency. For the case of 6-31G(d) basis set it is observed at 1.703 THz. This motion corresponds to the experimentally observed frequency at 1.57 THz. It should be noted here that experimental results of Bisphenol A (one of the ingredients for DGEBA) shows peaks at 1.69 THz as reported in literature [15].

Supplementary video related to this article can be found at https://doi.org/10.1016/j.biomaterials.2019.01.017.

3.2.6. 2.027 THz

Twisting about red axis of the aromatic ring could be observed from the numerical simulation configurations. For the case of 6-31G(d) basis set it is observed at 2.067 THz. This motion corresponds to the experimentally observed frequency at 1.95 THz.

Supplementary video related to this article can be found at https://doi.org/10.1016/j.biomaterials.2019.01.017.

3.2.7. 2.63 THz and 2.72 THz

Both of these correspond to the in and out motion of oxirane ring along the green axis (vertical axis in the plane of the paper). For the case of 6-31G(d) basis set it is observed at 2.669 THz. Both of these motions corresponds to the experimentally observed frequency at 2.6 THz.

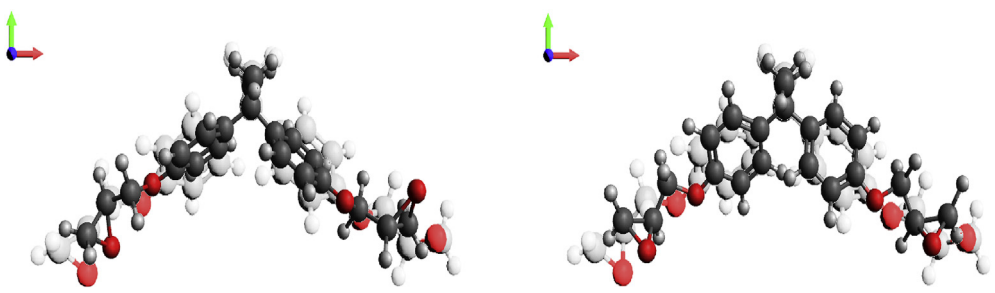

Fig. 10. 0.99 THz vibration configurations. Extremes of the deformed configurations are shown in bold and the initial undeformed configuration is shown in grey (in the background). Supplementary file (video 3) shows the animation of the molecules at 0.993 THz.

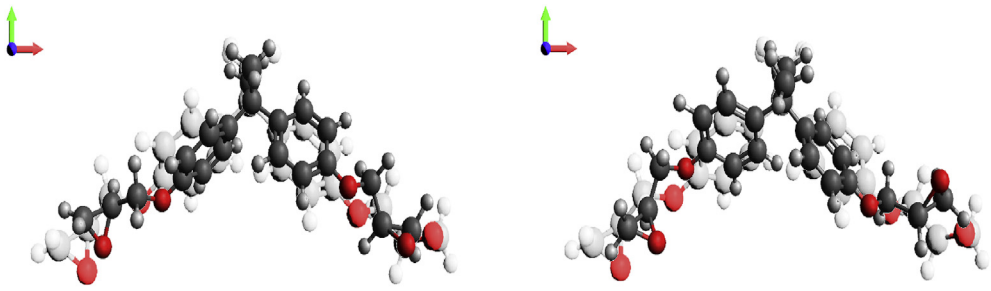

Fig. 11. 1.09 THz vibration configurations. Extremes of the deformed configurations are shown in bold and the initial undeformed configuration is shown in grey (in the background). Supplementary file (video 4) shows the animation of the molecules at 1.09 THz.

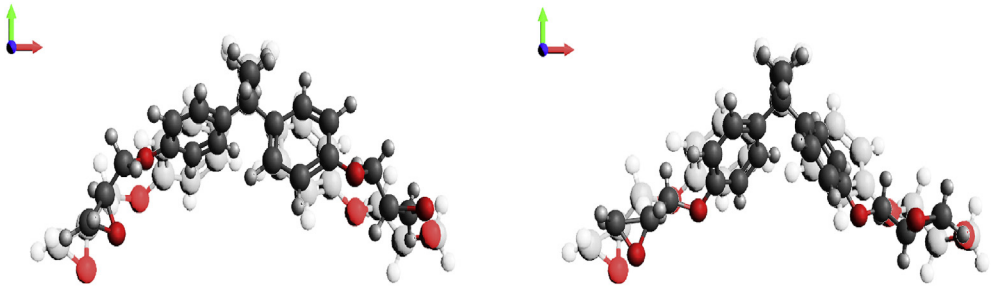

Fig. 12. 1.35 THz vibration configurations. Extremes of the deformed configurations are shown in bold and the initial undeformed configuration is shown in grey (in the background). Supplementary file (video 5) shows the animation of the molecules at 1.35 THz.

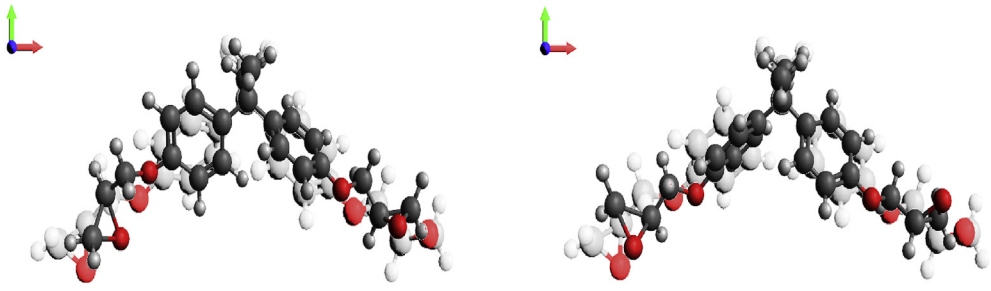

Fig. 13. 1.66 THz vibration configurations. Extremes of the deformed configurations are shown in bold and the initial undeformed configuration is shown in grey (in the background). Supplementary file (video 6) shows the animation of the molecules at 1.66 THz.

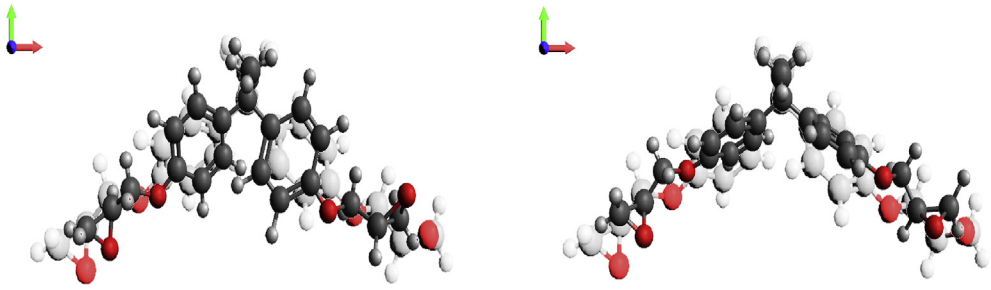

Fig. 14. 2.03 THz vibration configurations. Extremes of the deformed configurations are shown in bold and the initial undeformed configuration is shown in grey (in the background). Supplementary file (video 7) shows the animation of the molecules at 2.027 THz.

3.2.8. 2.63 THz

Supplementary video related to this article can be found at https://doi.org/10.1016/j.biomaterials.2019.01.017.

3.2.9. 2.72 THz

Supplementary video related to this article can be found at https://doi.org/10.1016/j.biomaterials.2019.01.017.

3.2.10. 2.99 THz

The absorption peak corresponds to twisting of CH_3–C–CH_3 bond about the red plane. For the case of 6-31G(d) basis set it is observed at 3.037 THz. This motion corresponds to the

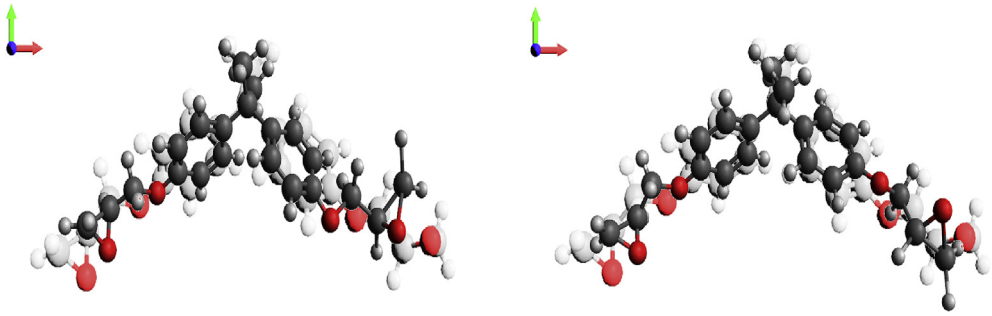

Fig. 15. 2.63 THz vibration configurations. Extremes of the deformed configurations are shown in bold and the initial undeformed configuration is shown in grey (in the background). Supplementary files (video 8) shows the animation of the molecules at 2.63 THz.

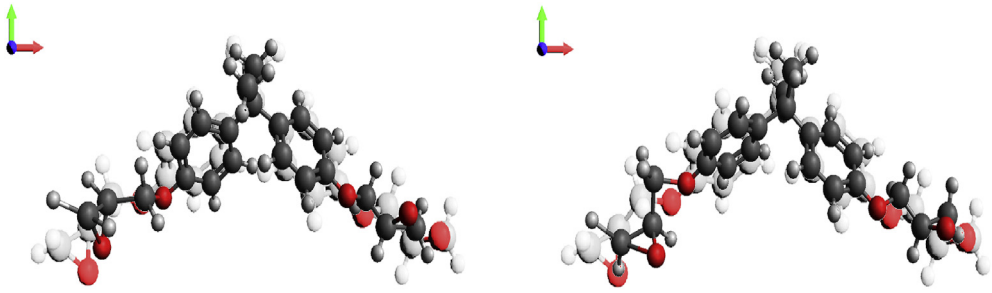

Fig. 16. 2.72 THz vibration configurations. Extremes of the deformed configurations are shown in bold and the initial undeformed configuration is shown in grey (in the background). Supplementary file (video 9) shows the animation of the molecules at 2.72 THz.

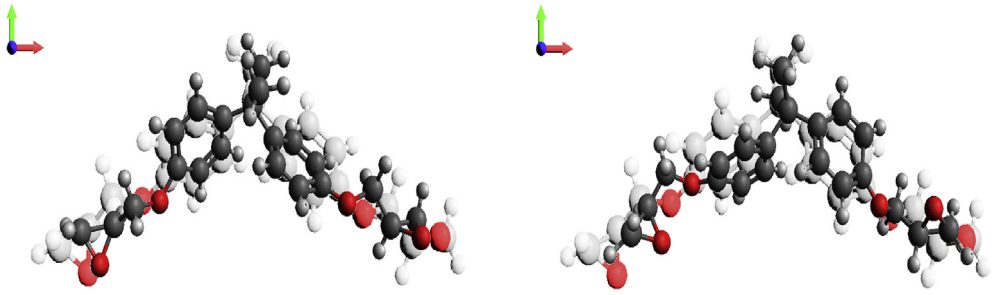

Fig. 17. 2.99 THz vibration configurations. Extremes of the deformed configurations are shown in bold and the initial undeformed configuration is shown in grey (in the background). Supplementary file (video 10) shows the animation of the molecules at 2.99 THz.

experimentally observed frequency at 2.9 THz.

Supplementary video related to this article can be found at https://doi.org/10.1016/j.biomaterials.2019.01.017.

Apart from the 2.26 THz observed experimentally, almost all the peaks observed experimentally could be simulated using the DFT simulations thereby explaining the corresponding motions associated with those absorption peaks. Obviously in some peaks there are differences in the frequencies observed experimentally and numerically, the reason for which have been discussed earlier in the manuscript.

4. Conclusions

Molecular vibrations of DGEBA, an important component of epoxy resin used in many different industries, is studied using a combination of Terahertz spectroscopy and Density Functional theory based calculations. The absorption peaks observed from experimental observations are correlated to that of vibrational motions of the entire molecule simulated by DFT calculation. It should be noted that the numerical study considered only a single molecule and thereby cannot simulate intermolecular vibrations. On the other hand, the experimental study is free from this limitation but since it is a commercially obtained material may have defects as well as other materials which might influence the vibration spectra. Thereby a combined experimental-numerical study of THz as well as DFT needs to be performed for development of a methodology to understand the molecular vibrational spectra especially at very low wavenumbers in which Infrared spectroscopy cannot be properly utilized.

Acknowledgement

Authors would like to acknowledge computational facilities at Prof. Mitra's lab and experimental facilities at Prof. Datta's lab.

Appendix A. Supplementary data

Supplementary data to this article can be found online at

https://doi.org/10.1016/j.molstruc.2019.01.094.

References

[1] D.C. Harris, M.D. Bertolucci, Symmetry and Spectroscopy: an Introduction to Vibrational and Electronic Spectroscopy, Dover Publications, 1989.
[2] M.A. González, J.L. Abascal, A flexible model for water based on tip4p/2005, J. Chem. Phys. 135 (22) (2011), 224516.
[3] N. Mitra, D. Prasad, S. Bandyopadhyay, Intermolecular dynamics of water: suitability of reactive interatomic potential, J. Chem. Phys., (submitted for publication).
[4] N. Mitra, D. Prasad, S. Banerjee, Identification of molecular vibrations associated with tacticity in polypropylene: density functional theory based simulations, J. Mol. Struct., (submitted for publication).
[5] H. Dannenberg, W. Harp, Determination of cure and analysis of cured epoxy resins, Anal. Chem. 28 (1) (1956) 86–90.
[6] K.E. Chike, M.L. Myrick, R.E. Lyon, S.M. Angel, Raman and near-infrared studies of an epoxy resin, Appl. Spectrosc. 47 (10) (1993) 1631–1635.
[7] P. Musto, L. Mascia, G. Ragosta, G. Scarinzi, P. Villano, The transport of water in a tetrafunctional epoxy resin by near-infrared fourier transform spectroscopy, Polymer 41 (2) (2000) 565–574.
[8] M.G. González, J.C. Cabanelas, J. Baselga, Applications of ftir on epoxy resins-identification, monitoring the curing process, phase separation and water uptake, in: Infrared Spectroscopy-Materials Science, Engineering and Technology, InTech, 2012.
[9] M.J. Frisch, G.W. Trucks, H.B. S, et al., Gaussian09 Revision E.01, gaussian Inc., Wallingford CT, 2009.
[10] A.D. Becke, A new mixing of Hartree–Fock and local density-functional theories, J. Chem. Phys. 98 (2) (1993) 1372–1377.
[11] C. Lee, W. Yang, R.G. Parr, Development of the colle-salvetti correlation-energy formula into a functional of the electron density, Phys. Rev. B 37 (2) (1988) 785.
[12] J.P. Perdew, M. Ernzerhof, K. Burke, Rationale for mixing exact exchange with density functional approximations, J. Chem. Phys. 105 (22) (1996) 9982–9985.
[13] A.C. Das, S. Bhattacharya, M. Jewariya, S.S. Prabhu, K.C. Mandal, T. Ozaki, P.K. Datta, Identification of combination phonon modes in pure and doped GaSe crystals by THz spectroscopy, IEEE J. Sel. Top. Quantum Electron. 23 (4) (2017) 1–7.
[14] P.U. Jepsen, D.G. Cooke, M. Koch, Terahertz spectroscopy and imaging–modern techniques and applications, Laser Photon. Rev. 5 (1) (2011) 124–166.
[15] R. Ullah, H. Li, Y. Zhu, Terahertz and ftir spectroscopy of bisphenol a, J. Mol. Struct. 1059 (2014) 255–259.
[16] E. Fedulova, M.M. Nazarov, A. Angeluts, M. Kitai, V. Sokolov, A. Shkurinov, Studying of dielectric properties of polymers in the terahertz frequency range, in: Saratov Fall Meeting 2011: Optical Technologies in Biophysics and Medicine XIII, vol. 8337, International Society for Optics and Photonics, 2012, p. 83370I.
[17] P. Atkins, J. de Paula, Atkins' Physical Chemistry, OUP, Oxford, 2010.